Boundary Layer Depth, Entrainment, and Decoupling in the Cloud-Capped Subtropical and Tropical Marine Boundary Layer

ROBERT WOOD AND CHRISTOPHER S. BRETHERTON

University of Washington, Seattle, Washington

(Manuscript received 8 September 2003, in final form 9 February 2004)

ABSTRACT

Estimates of marine boundary layer (MBL) depth and degree of decoupling for two regions of the subtropical and tropical east Pacific are presented using satellite observations from the Moderate Resolution Imaging Spectroradiometer (MODIS) and the Tropical Rainfall Measuring Mission (TRMM) Microwave Imager (TMI). These data are combined in a novel way with NCEP reanalysis data and a mixing line parameterization to estimate the mean entrainment rate w_e over the two regions. Mean entrainment rates vary geographically and have maxima just downwind of the Californian coast ($\overline{w_e} \approx 4$–5 mm s^{-1}), and also in the core of the equatorial east Pacific cold tongue where mean w_e exceeds 6 mm s^{-1}. Entrainment exceeds subsidence by 30% or less in the subtropical stratocumulus regions. North of the equatorial cold tongue entrainment greatly exceeds subsidence, producing a rapid deepening of the MBL as air flows over a marked SST gradient.

Shallow MBLs ($z_i < 500$–700 m) are found to be well mixed in general. The decoupling increases markedly for deeper boundary layers and is well parameterized as a function of the thickness of the layer extending from the top of the surface mixed layer to the MBL inversion. This study demonstrates new ways in which large-scale observational and reanalysis datasets may be used to aid understanding of MBL boundary layer and cloud systems.

1. Introduction

It is important that regional and global numerical models can simulate accurately the processes occurring in the cloud-topped marine boundary layer (MBL). The entrainment rate w_e is a crucial parameter for the evolution of cloud thickness because it determines the magnitude of the warming and drying of the MBL by incorporation of free tropospheric air (Lilly 1968; Deardorff 1976). Entrainment is notoriously difficult to measure (see, e.g., Stevens et al. 2003a). If methods of making estimations of the entrainment rate at the regional scale can be developed they will provide an excellent constraint for the wealth of entrainment closures in existence (see, e.g., the reviews in Nicholls and Turton 1986 and Stevens 2003).

Direct observations of the MBL depth z_i over the World Ocean are sparse and may not be representative of climatological values. The first attempts at producing a climatology of z_i in regions dominated by low cloud were produced using aircraft over the North Atlantic (von Ficker 1936; see review by Kloesel 1992), and subsequently over the subtropical northeast (NE) Pacific by Neiburger et al. (1961) using shipborne radiosonde ascents. These studies are pioneering, but limited, because they comprise only a relatively small number of observations. Initial attempts have been made to use the wealth of available satellite data to produce climatologies of MBL depth that could prove valuable in determining the links between MBL depth, decoupling, and cloud cover. For example, a 5-yr climatology of mean MBL depth has been derived from geostationary satellite data (Heck et al. 1990) and has been used to validate a regional model simulation (Wang et al. 1993). Minnis et al. (1992) estimated boundary layer depths in the NE Pacific using a fixed lapse rate between the sea surface temperature and the cloud-top temperature. More recent observations have found that deeper boundary layers tend to be more decoupled than shallow ones, suggesting that the constant lapse-rate assumption is inappropriate over much of the subtropical ocean. Betts et al. (1992) combined a simple mixing line parameterization with observations of cloud-top temperature to estimate z_i in the NE Pacific.

It is commonly observed that the MBL does not remain well mixed when it deepens downwind of the subtropical stratocumulus regions (e.g., Albrecht et al. 1995; Betts et al. 1995). One of the major hypotheses to describe the important transition from stratocumulus to cumulus cloud over the subtropical oceans states that the deepening of the MBL through entrainment is a key process leading to decoupling and a subsequent reduc-

Corresponding author address: Dr. Robert Wood, Atmospheric Sciences, University of Washington, Box 351640, Seattle, WA 98195. E-mail: robwood@atmos.washington.edu.

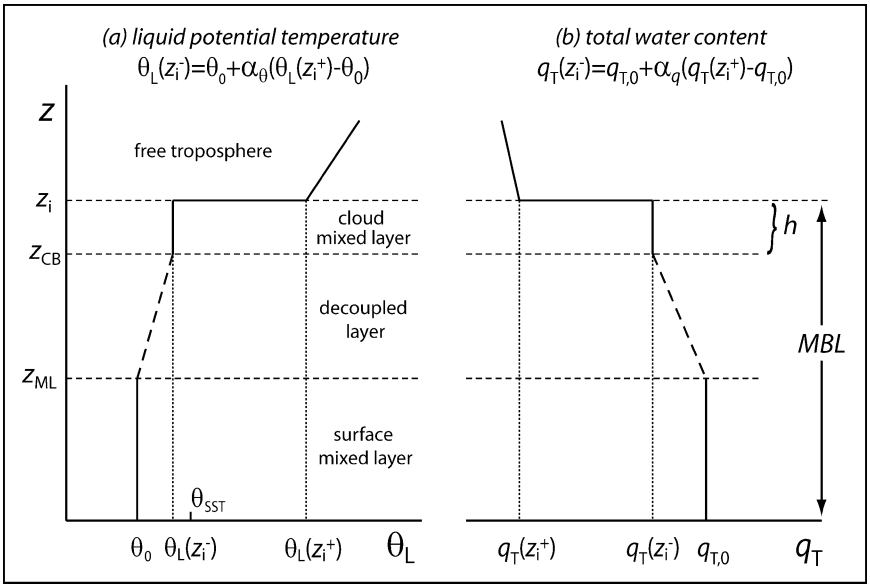

FIG. 1. MBL structure for (a) liquid potential temperature θ_L and (b) total water content q_T assumed in this study, following PLR, with separate decoupling parameters α_θ and α_q. Refer to the main text for a description of the parameters. The dashed lines indicate where the Park model does not explicitly specify the profiles.

tion in cloud cover (Bretherton and Wyant 1997). Observations that provide support for the warming-deepening hypothesis are generally limited to specific detailed observational case studies (Bretherton and Pincus 1995; de Roode and Duynkerke 1997; Klein 1997; Osborne et al. 2000).

In this study we combine satellite observations of cloud-top temperature, sea surface temperature, and cloud liquid water path with National Centers for Environmental Prediction–National Center for Atmospheric Research (NCEP–NCAR) reanalysis data (Kistler et al. 2001) using a novel method to estimate boundary layer depth, entrainment rate, and decoupling in the cloud-capped MBL. The methodology is outlined in section 2. Results are presented in section 3, and conclusions in section 4. An appendix provides details of our analysis of the possible uncertainties involved in the estimates.

2. Methodology

We consider two study regions. The first (10°–50°N, 150°–110°W) covers the NE Pacific subtropical region including the transition from near coastal, shallow, stratus-capped MBLs to deeper trade wind cumulus-capped boundary layers to the west. The second region (30°S–10°N, 120°–70°W) covers the southeast Pacific subtropical region and the east Pacific cold tongue region. In both regions the dominant clouds are found in the boundary layer (see, e.g., Fig. 1 in R. Wood and D. L. Hartmann 2004, unpublished manuscript, hereafter WaH). Two complete months of data are used (September–October 2000).

a. Entrainment rate

The MBL depth z_i is given by

$$\frac{\partial z_i}{\partial t} + \mathbf{u}(z_i)\cdot\nabla z_i = w_e - w_s(z_i), \tag{1}$$

where $\mathbf{u}(z_i)$ is the horizontal wind velocity, w_e is the entrainment rate, and $w_s(z_i)$ is the subsidence rate, at z_i. Our goal is to determine the climatological mean value of w_e using a combination of satellite estimations of z_i and NCEP reanalysis values of $w_s(z_i)$. Taking the mean of (6) over a long enough period that $\partial z_i/\partial t = 0$, we obtain

$$\overline{w_e} = \overline{\mathbf{u}(z_i)\cdot\nabla z_i} + \overline{w_s(z_i)}. \tag{2}$$

The first term on the rhs of (2) can be simplified to a vector product of mean quantities provided that $\overline{\mathbf{u}'(z_i)\cdot\nabla z_i'} \ll \overline{\mathbf{u}(z_i)}\cdot\nabla\overline{z_i}$. We consider that this assumption is valid because (i) the synoptic wind speed variability (σ_u) is everywhere less than 50% of the mean in our study regions, and (ii) ∇z_i variations are found to be typically much smaller than the time mean ∇z_i.

Then, (2) becomes

$$\overline{w_e} \approx \overline{\mathbf{u}(z_i)}\cdot\nabla\overline{z_i} + \overline{w_s(z_i)}. \tag{3}$$

The time mean is over the shortest averaging time scale for which we are able to obtain a reasonably noise-free z_i average, which is 2 months. The following sections detail our method for estimation of the terms in (3), and an assessment of the uncertainties associated with the analysis are presented in the appendix.

b. Estimation of MBL depth

MBL depth is estimated using the observed temperatures of the sea surface (SST) and the cloud top T_{top}, and the observed liquid water path (LWP) of the clouds. The MBL is assumed to take the structure presented in Park et al. (2004, manuscript submitted to *J. Atmos. Sci.*, hereafter PLR), which is a variant of the mixing line model first introduced by Betts (1985; see Fig. 1).

Observations of T_{top} are from the Moderate Resolution Imaging Spectroradiometer (MODIS) situated on the National Aeronautics and Space Administration (NASA) *Terra* satellite (King et al. 1992). Our analysis is carried out on 256 km $\times$ 256 km scenes that are a subset of each MODIS data granule (see WaH). This is large enough that almost all scenes contain some warm cloud from which to estimate the MBL cloud-top temperature, but small enough that we can capture regional variability in z_i. We only use scenes containing exclusively warm cloud. Approximately 30 000 such scenes are analyzed to produce the 2-month dataset. We use only daytime data ($\sim$1030 local time) from MODIS because we require retrievals of optical thickness and effective radius in order to estimate the cloud liquid water path (Nakajima and King 1990; King et al. 1997). The use of only daytime data could introduce biases in derived climatologies because of the strong diurnal cycle in z_i that can occur in the subtropical cloud-capped boundary layer. We discuss this further in section 3.

Measurements of SST are taken from the Tropical Rainfall Measuring Mission (TRMM) microwave imager (TMI). Details of the instrument are given in Kummerow et al. (1998). The SST corresponding to each MODIS scene is estimated by spatial interpolation from 3-day maps of SST produced by Remote Sensing Systems (Wentz 1997).

For optically thick MBL clouds, the satellite-measured cloud-top temperature T_{top} is close to the temperature just below the MBL inversion base $T(z_i^-)$. Our analysis therefore will result in an assessment of the MBL depth and entrainment rate in cloudy boundary layers, and cannot be used to speculate upon the role of clear-sky entrainment.

Additional assumptions about the MBL temperature structure are required to estimate z_i for each MODIS scene (see Fig. 1a): (i) there is a surface mixed layer (SML) from the ocean surface to the surface-derived lifted condensation level (LCL) z_{ML}; (ii) the liquid potential temperature θ_L is stratified from z_{ML} up to the mean cloud-base height z_{CB} [the decoupled layer (DL)], with a moist-adiabatic cloud layer of thickness h below the MBL inversion. The mean DL stratification (but not the precise shape of the profile) is parameterized using the PLR formulation, which effectively specifies the slope of the mixing line in the Betts (1985) approach. The parameterization can be stated as

$$\theta_L(z_i^-) = \theta_0 + \alpha_\theta[\theta_L(z_i^+) - \theta_0], \tag{4}$$

where θ_0 is the SML potential temperature, and α_θ is a parameter that expresses the degree of stratification of the θ_L profile (the ''decoupling'' parameter). The total water mixing ratio q_T has an analagous decoupling relation

$$q_T(z_i^-) = q_{T,0} + \alpha_q[q_T(z_i^+) - q_{T,0}], \tag{5}$$

where $q_T(z_i^-)$, $q_T(z_i^+)$, and $q_{T,0}$ are the total water mixing ratios just below the inversion, just above the inversion, and in the SML.

Following PLR, we make the assumption that the decoupling parameters are related via $\alpha_\theta = (1 - a\text{CF})\alpha_q$, where CF is the (MODIS-derived) cloud fraction, and $a = 0.2$. This is a simple parameterization, described in PLR, based upon the idea that the ratio of decoupling parameters α_θ/α_q is governed by cloud-top radiative cooling to first order. Combination of (4), (5), and the relationship between α_θ and α_q, together with an expression relating θ_L to θ (e.g., Bolton 1980), leads to an equation for z_i

$$\frac{T_{\text{top}}}{\Pi(z_i)}\exp\left(-\frac{L_v q_{L,i}}{c_p T_{\text{top}}}\right) = \theta_0 + [\theta_L(z_i^+) - \theta_0](1 - a\text{CF}) \times \left[\frac{q_T(z_i^-) - q_{T,0}}{q_T(z_i^+) - q_{T,0}}\right], \tag{6}$$

where $q_{L,i}$ is the liquid water mixing ratio at the top of the (adiabatic) cloud layer, L_v is the latent heat of condensation of water (assumed constant at its 293 K value), c_p is the specific heat capacity of air at constant pressure, and $\Pi(z)$ is the Exner function at height z (pressure p). The SML potential temperature is given by

$$\theta_0 = (\text{SST} - \Delta T_{S-A})\Pi_0^{-1}, \tag{7}$$

where ΔT_{S-A} is the sea–air temperature difference, and Π_0 is the surface Exner function. We assume, for each MODIS scene, that ΔT_{S-A} is equal to its September–October climatological value for the scene location, determined from the Comprehensive Ocean–Atmosphere Data Set (COADS; Woodruff et al. 1998). These climatological data are also used to provide estimates of the surface relative humidity RH_0, which is used along with θ_0 and the surface pressure p_0 to derive z_{ML}. Surface pressure is taken from the NCEP reanalysis.

We use the adiabatic assumption to relate $q_{L,i}$ to LWP, that is, $q_{L,i} = (2\text{LWP}\ \Gamma_{\text{ad}})^{1/2}$ (e.g., Wood and Taylor 2001), where Γ_{ad} is a weak function of temperature and pressure that is assumed to be constant within the cloud layer. The value of LWP used to obtain $q_{L,i}$ is the MODIS mean LWP of all the cloudy pixels within a scene. The LWP measurements also provide a measure of the cloud thickness h, through $\text{LWP} = (1/2)\Gamma_{\text{ad}}h^2$. This thickness is used to estimate $q_T(z_i^-)$ because for an adiabatic cloud layer $q_T(z_i^-) = q_{\text{sat}}(T_{\text{CB}}, p_{\text{CB}})$, where $q_{\text{sat}}(T, p)$ is the saturation specific mixing ratio, and T_{CB} and p_{CB} are the cloud-base temperature and pressure, respectively. The

cloud-base temperature is obtained via $T_{CB} = T_{top} + \Gamma_m h$, where Γ_m is the moist-adiabatic lapse rate. The cloud-base pressure is estimated using a simple scale–height relation.

NCEP reanalysis data are used to specify free-tropospheric conditions. We use the NCEP 700-hPa temperature interpolated in time and space for each MODIS scene, and a specified free-tropospheric stratification $\Gamma_{FT} = d\theta/dz = 5$ K km^{-1} between the 700-hPa level and z_i to determine $\theta_L(z_i^+)$. The free-tropospheric lapse rate is largely determined by radiatively driven subsidence and does not exhibit large variability in the Tropics (see e.g., Betts and Ridgway 1988) and subtropics. We find from East Pacific Investigation of Climate Processes in the Coupied Ocean–Atmosphere System (EPIC) data (Bretherton et al. 2003) and other subtropical data (Albrecht et al. 1995) that values of $d\theta/dz$ in the subtropics are similar to those found in the Tropics. NCEP reanalysis q_T at 700 hPa is used to provide $q_T(z_i^+)$, as observations from EPIC and elsewhere typically reveal relatively weak vertical moisture gradients in the first 2–3 km of the free-troposphere (Betts and Albrecht 1987; Albrecht et al. 1995). The COADS surface relative humidity climatology (September–October 1960–95) is used to obtain $q_{T,0}$. We examine the sensitivity of our results to these assumptions in the appendix.

An interative solution is implemented to solve (6) for z_i, using Müller's method, for each MODIS scene, with the additional assumption that the pressure profile $p(z)$ can be expressed using a simple scale–height formulation. The results are insensitive to the exact choice of pressure–height relationship used. This method is similar to that used by Betts et al. (1992), except that in this study the observed LWP is an additional constraining parameter, which means that the decoupling parameter α_q (or equivalently the slope of the mixing line in the Betts formulation) is an additional output parameter, which we will investigate in this study. We examine the uncertainties in α_q in the appendix.

For comparison purposes, solutions for z_i of (6), assuming that the MBL is well mixed throughout its depth, are obtained by forcing the decoupling parameter to be zero and setting the cloud depth equal to $z_i - z_{ML}$. The MODIS LWP observations are not used in this case. The sensitivity of z_i to the model assumptions is discussed in the appendix.

c. Subsidence at the MBL top

Subsidence rates are estimated from NCEP reanalysis. For each MODIS scene, we estimate the 850-hPa subsidence rate using the 850-hPa NCEP pressure velocity ω interpolated to the location of the scene. To remove diurnal effects, we derive the mean value of ω for the 24 h centered on the MODIS scene time. Tidal and other pressure tendency effects are removed by subtracting the surface pressure velocity, which is an appropriate method in the lowest few kilometers of the troposphere. To estimate $\omega_s(z_i)$ we assume that large-scale lower-tropospheric divergence D is constant over the lower troposphere, so that $\omega_s(z_i) = \omega_s(850\text{ hPa})z_i/z_{850\text{hPa}}$. Analysis of the NCEP reanalysis fields suggests that this is an appropriate assumption throughout most of the subtropics and divergent Tropics.

d. Downstream deepening of z_i

The ''downstream deepening'' (Eulerian advection) of z_i is estimated as $\mathbf{u}(z_i) \cdot \nabla\overline{z_i}$. The z_i gradient vector is estimated by first smoothing the $2.5^\circ \times 2.5^\circ$ gridded z_i data with a 1-2-1 filter, followed by centered differencing. The mean wind velocity at z_i is obtained from NCEP reanalysis by interpolation to z_i. Almost everywhere throughout the undisturbed subtropics north of 15°N and south of 5°S, there is little wind shear in the lower troposphere, and so the interpolated wind velocity $\mathbf{u}(z_i)$ is reasonably close to that at 925 or 850 hPa. However, toward the intertropical convergence zone (ITCZ) there can be considerable wind shear and the interpolation procedure is likely to be more accurate.

3. Results

a. Boundary layer depth

Mean z_i for the 2-month period is shown in Figs. 2a and 3a. Inversion-level winds are also shown. Shallow MBLs exist in the upwelling regions close to the coasts, and these deepen with distance downwind as the boundary layer moves westward and equatorward, and transitions from a well-mixed stratus/stratocumulus-capped boundary layer into a decoupled trade wind boundary layer (Bretherton and Wyant 1997). This general deepening of the MBL away from the coastal regions is in agreement with the observations of Neiburger et al. (1961). The deepest boundary layers are found equatorward and westward in the trade wind belts, and compare favorably here with the observations of Riehl et al. (1951). In the SE Pacific, where measurements are sparse, the results agree quite favorably with results from a recent ship cruise (Garreaud et al. 2001) which show shallow MBLs ($z_i < 1000$ m) near the Chilean coast at 27°S that deepen westward to around 2000 m in the trades at 27°S, 110°W. If one assumes that the boundary layer is well mixed to derive z_i, then the deeper trade wind boundary layers tend to be 500–1000 m too shallow (see the appendix), which lends support to the PLR formulation.

Liquid water paths consistent with the mixed-layer solutions are generally much greater than those observed, especially for deeper z_i. In contrast to these mixed-layer solutions, the observations do not show a strong correlation of LWP with z_i (WaH). The median overprediction of LWP by the mixed layer model is 430%, but is much less for shallow boundary layers, with almost no overprediction for $z_i < 1000$ m, and an

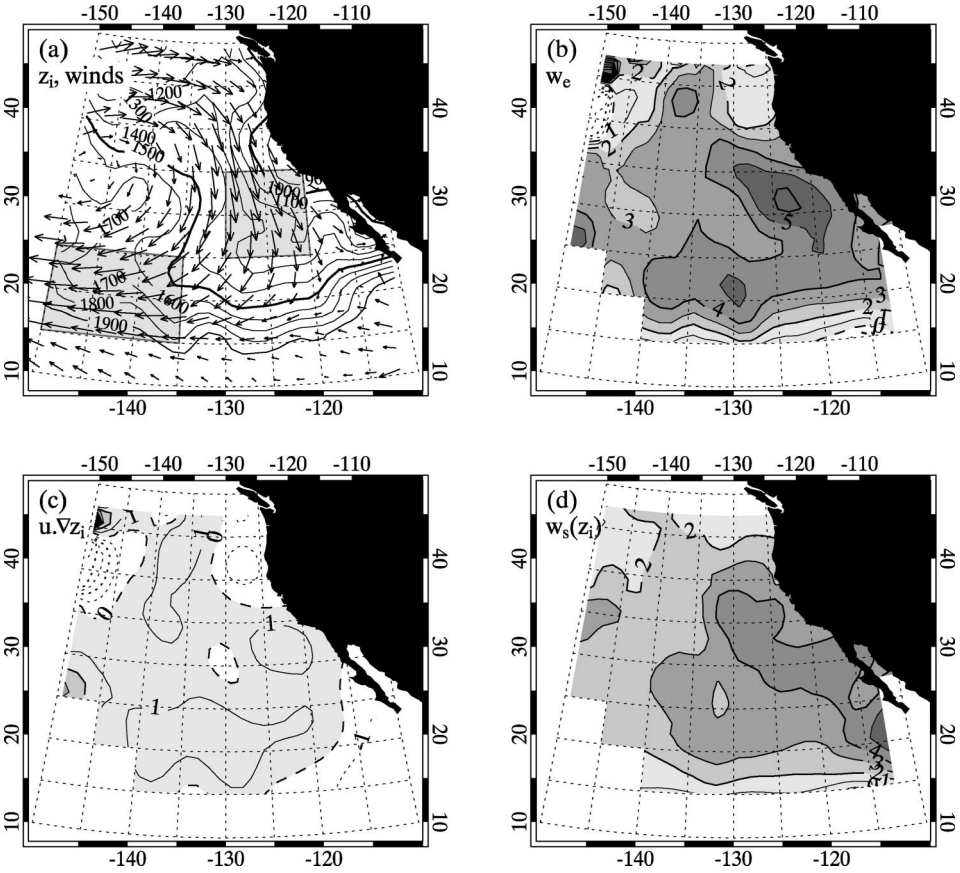

FIG. 2. NE Pacific (a) MBL depth z_i (contours) and inversion height mean wind $\overline{\mathbf{u}(z_i)}$. Shaded regions show specific regions identified in the text; (b) mean derived entrainment rate $\overline{w_e}$ (mm s^{-1}); (c) downstream deepening rate $\overline{\mathbf{u}(z_i)} \cdot \nabla \overline{z_i}$ (mm s^{-1}); (d) mean inversion height subsidence rate $w_s(z_i)$ (mm s^{-1}). (b)–(d) Shaded regions indicate values greater than 2 mm s^{-1}.

overprediction of an order of magnitude for $2000 < z_i < 2500$ m. This suggests that the assumption that the MBL is well mixed becomes inconsistent with observations when the MBL deepens beyond approximately 1 km. Results from time-evolving mixed-layer simulations forced with realistic boundary conditions (Wakefield and Schubert 1981) show a similar pattern, with cloud thicknesses (and therefore LWP) that are much larger than observations when the MBL is deeper than around 800 m.

The MBL along the South American coast is generally 100–200 m deeper than those close to the Californian coast. This is probably related to differences in orography along the two coastlines. Another interesting difference is that over a considerable area of the SE Pacific, the inversion-level winds are directed along contours of constant z_i. To the north of the equatorial cold tongue, the MBL deepens rapidly in response to strong surface forcing.

Minnis et al. (1992) used a fixed lapse rate of 7.1 K km^{-1} between the SST and T_{top} to estimate the MBL depth over the NE Pacific. We compare this lapse rate with our estimates (Fig. 4). We find that the lapse rate $(\text{SST} - T_{\text{top}})/z_i$ in units of K km^{-1} is well parameterized as a function of z_i itself

$$\frac{\text{SST} - T_{\text{top}}}{z_i} = 9.2 \exp\left[-\left(\frac{z_i}{4800}\right)^2\right]. \qquad (8)$$

Our values compare quite well with those of Betts et al. (1992) using a mixing line parameterization, who found lapse rates in the range 7–8.5 K km^{-1} over the NE Pacific. Given only observations of SST and T_{top}, it is possible to solve (8) to obtain more accurate estimates of z_i than those assuming a constant lapse rate.

b. Entrainment-rate climatology

Figures 2b–d and 3b–d show maps of parameters associated with the diagnosis of entrainment rate. Table 1 shows mean values for the five shaded subregions. Uncertainties in $\overline{w_e}$ are estimated at around 25% of the mean for the NE Pacific and 40% for the SE Pacific (see appendix). Uncertainties in z_i are rough estimates based upon the possible biases, sampling errors, and

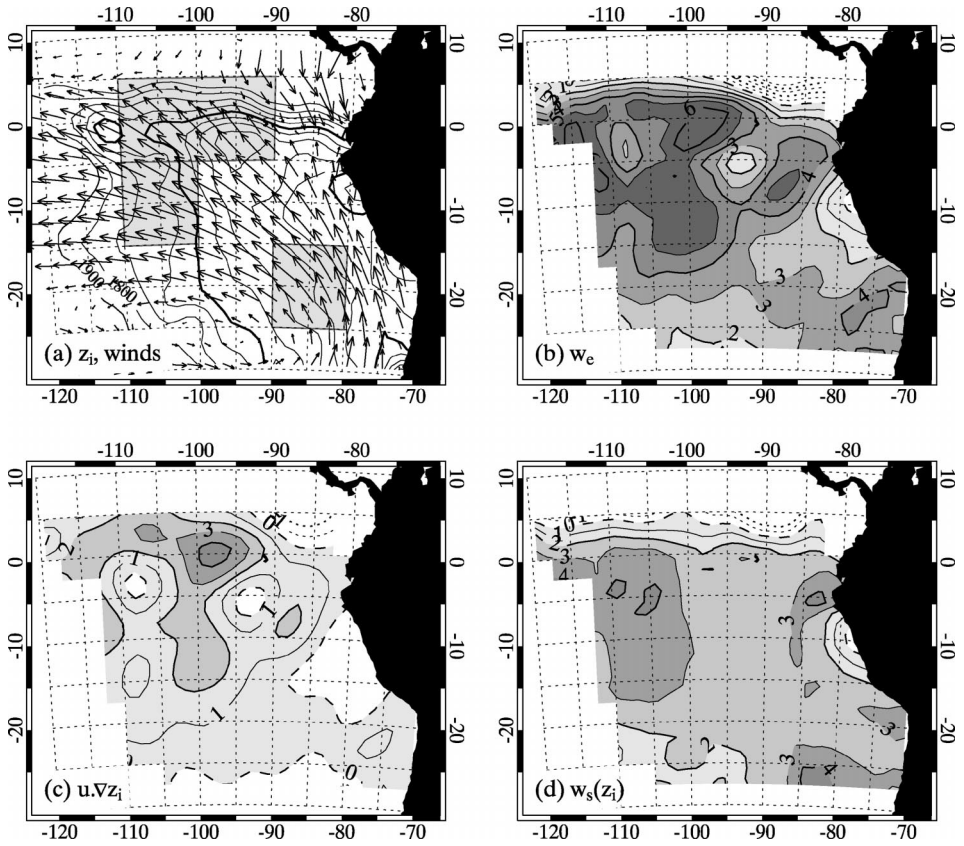

FIG. 3. As in Fig. 2 but for the SE Pacific region.

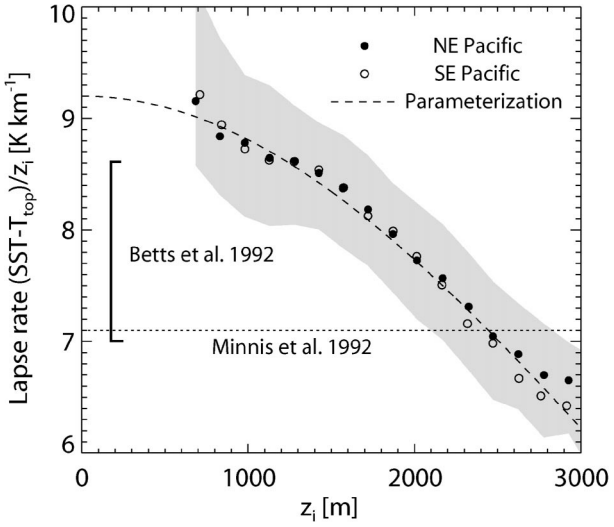

FIG. 4. Lapse rate, defined as (SST $-$ T_{top})/z_i estimated from the analysis in this study, binned as a function of z_i. The shaded region shows the 10th and 90th percentiles and the dashed line shows the parameterization (8).

uncertainties in the PLR model discussed in the appendix.

Throughout the subtropical stratocumulus and trade wind regions, the downstream deepening is typically less than 30% of the entrainment rate, depending upon the degree of cold advection. This approximate balance between entrainment and subsidence has been observed in recent in situ field studies (Faloona et al. 2004, manuscript submitted to *J. Atmos. Sci.*, hereafter FAL) and is particularly evident in our estimates in the SE Pacific stratocumulus region, where downstream deepening is small. An important exception is the region to the north of the E Pacific equatorial cold tongue where the mean entrainment rate is as large as a factor of 2 greater than the mean subsidence rate. This imbalance is caused by the strong surface forcing in the cross-equatorial MBL (McGauley et al. 2004; deSzoeke and Bretherton 2004) as cold air flows over a strong SST gradient, causing sharp increases in surface fluxes and an associated increase in the turbulent mixing in the MBL.

The mean entrainment values can be considered as diurnal mean values because (a) we used daily mean values of the subsidence rate for each scene; (b) although the mean z_i is only valid at the 1030 local time corresponding to the MODIS overpasses, the diurnal cycle of the the downstream deepening is likely to be

TABLE 1. Entrainment rate, subsidence rate, downstream deepening rate, and MBL depth for the five subregions examined.

Subregion	Lon	Lat	$\overline{w_e}$ (mm s^{-1})	$\overline{w_s}$ (mm s^{-1})	$\overline{\mathbf{u}\,(z_i)\cdot\nabla z_i}$ (mm s^{-1})	$\overline{z_i}$ (m)
a. NE Pacific Sc	120°–130°W	25°–35°N	4.8 ± 1.2	4.1 ± 0.8	0.8 ± 0.2	1200 ± 100
b. NE Pacific trade Cu	135°–150°W	15°–25°N	3.2 ± 0.8	2.1 ± 0.4	1.1 ± 0.3	1730 ± 250
c. SE Pacific Sc	80°–90°W	15°–25°S	2.7 ± 1.2	2.6 ± 0.9	0.1 ± 0.1	1140 ± 100
d. SE Pacific trade Cu	100°–110°W	5°–15°S	5.3 ± 2.0	3.4 ± 1.2	2.0 ± 0.5	1560 ± 200
e. Equatorial	90°–110°W	5°S–5°N	4.8 ± 1.0	2.5 ± 0.8	2.5 ± 0.7	1535 ± 200

small. Given that at most subtropical locations the MBL is close to its mean height at the MODIS overpass time (1030 local time), we do not expect that the diurnal cycle of z_i will strongly affect the estimation of the subsidence rate at the MBL top.

The values of $\overline{w_e}$ should not be considered as all-time means, because those scenes containing non-MBL cloud have been excluded from the analysis. The values are representative of mean entrainment rates when only MBL clouds are present. The fraction of excluded scenes is typically 10%–40% in the subtropics, increasing to over 60% in the tropical and midlatitude regions (WaH), although it should be noted that around 5% of scenes are rejected for technical reasons related to optical depth retrieval error (these are flagged and so easily rejected) rather than because non-MBL clouds are present.

Mean w_e in the subtropical stratocumulus and trade wind regions is 2–6 mm s^{-1}. Recent in situ observations in the NE Pacific stratocumulus region (FAL) give a mean value consistent with our results. There appears to be a decrease in $\overline{w_e}$ as the cloud type decreases from overcast (stratocumulus) to broken (trade cumulus) in the NE Pacific, but an increase in the SE Pacific. This could reflect geographical differences in either the strength of the turbulence or the MBL inversion strength in the two regions. Through the transition from stratocumulus to cumulus the inversion strength weakens (favoring entrainment) but the overall level of turbulence decreases (opposing entrainment). The evolution of w_e depends sensitively upon the balance between the two opposing changes. Extension of this type of climatology to other seasons could shed additional light on the factors controlling w_e. Also of note is that $\overline{w_e}$ for the NE Pacific stratocumulus region is around 50% higher than for the stratocumulus region in the SE Pacific (see Table 1). This may reflect differences in the strength of the temperature and/or moisture inversions in the two regions.

TABLE 2. Median values of α_θ, α_q, and cloud fraction (CF), for the five regions detailed in Table 1.

Subregion	α_θ	α_q	CF
a	0.15 ± 0.08	0.18 ± 0.06	0.70
b	0.30 ± 0.10	0.32 ± 0.08	0.31
c	0.11 ± 0.07	0.13 ± 0.06	0.85
d	0.24 ± 0.08	0.27 ± 0.08	0.50
e	0.29 ± 0.08	0.33 ± 0.07	0.64

To the north of the E Pacific cold tongue, $\overline{w_e}$ is typically 4–7 mm s^{-1}. The observed peak in $\overline{w_e}$ is approximately on the equator (Fig. 3), whereas it would be expected to be 2°–3° farther north based upon the observed location of the sharp SST front that marks the northerly edge of the tongue (Thum et al. 2002). This displacement is primarily due to the smoothing of the observed z_i field close to a region where there is a sharp gradient (i.e., north of the equator). This smoothing smears out the peak entrainment rate. The true maximum north of the cold tongue may actually be considerably higher in magnitude, and more narrow in latitudinal extent than is represented in Fig. 3.

c. Decoupling

Uncertainties in the estimation of the decoupling parameter α_q are addressed in the appendix. Estimated rms uncertainties are 0.1–0.13 for α_q and α_θ. Table 2 gives estimated median values of α_θ and α_q for the five subregions. Figure 5 shows a joint probability density function (PDF) of α_q and the DL depth $z_i - z_{ML}$ with data taken from the NE Pacific MODIS scenes. The SE Pacific data are very similar. The data show that the de-

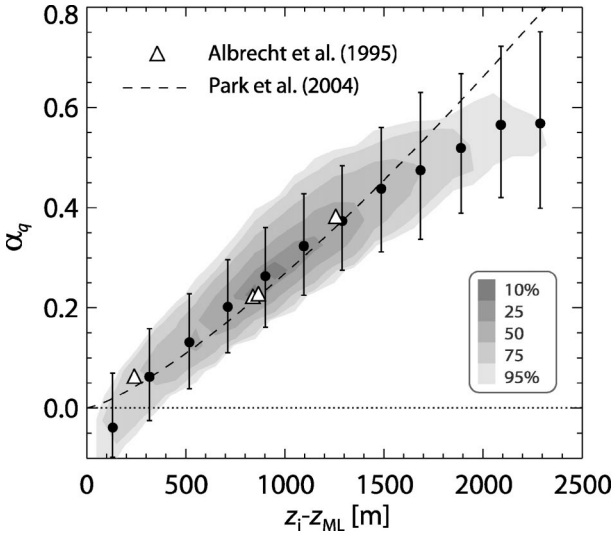

FIG. 5. (a) Joint PDF of α_q and decoupled layer depth $z_i - z_{ML}$ with dashed line showing PLR model parameterization. Open triangles show values derived from the observational results of Albrecht et al. (1995) assuming that $z_{ML} = 475$ m, the median value for the NE Pacific data. Bars show estimated errors.

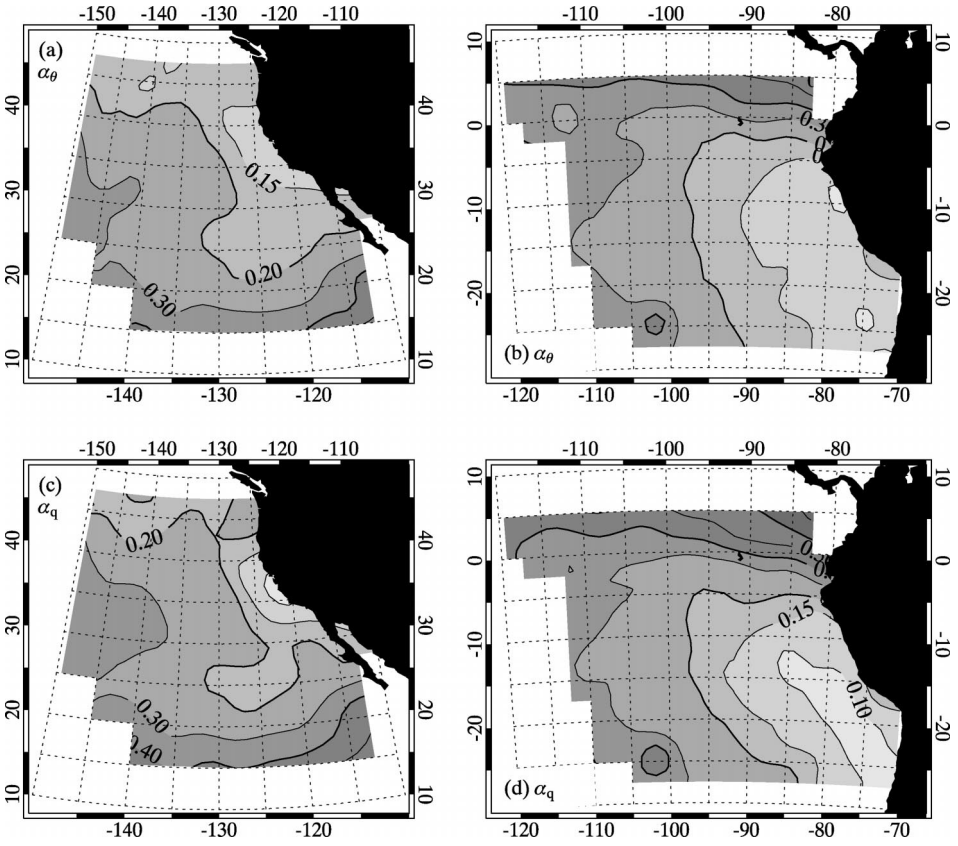

FIG. 6. Median values of (a), (b) α_θ and (c), (d) α_q for the NE and SE Pacific regions. Contours are every 0.05.

coupling parameter is well parameterized as a function of $z_i - z_{\mathrm{ML}}$. The suggested parameterization presented in PLR agrees with the data to within the estimated uncertainty, although there is a suggestion of overprediction by PLR for the shallowest and deepest z_i. Observational estimates from Albrecht et al. (1995) for four MBL datasets also agree well with the data. The negative values of α_q in the data result from cases where the solution to (6) gives $z_i - z_{\mathrm{ML}}$ smaller than the adiabatic cloud thickness corresponding to the observed LWP. Approximately 6% of cases have this condition, which results from uncertainties in z_i (see appendix) or uncertainties in the estimation of z_{ML} which is largely determined by climatology in our study.

Maps of the median values of α_θ and α_q are shown in Fig. 6. The degree of decoupling is smallest closest to the coasts ($\alpha_q \sim 0.1$–0.15), where we find the shallowest and most overcast boundary layers. There is a general transition to more decoupled MBLs in the deeper trade wind MBL ($\alpha_q = 0.2$–0.4). This agrees qualitatively with the decoupling hypothesis of Bretherton and Wyant (1997), in which the stratocumulus to trade cumulus transition is directly linked to the deepening boundary layer over warmer seas. Interestingly, although the shallowest MBLs of all are found closest to the Californian coast, the smallest values of α_q are found in the SE Pacific. This might be a hint that, in reality, the degree of decoupling may not simply be a function of the decoupled layer depth, but might be affected by other large-scale processes such as drizzle. We leave this possibility open for future study.

4. Conclusions

In this study we have attempted to estimate mean entrainment rates for the subtropical and tropical MBL over the east Pacific Ocean, using a combination of satellite observations and NCEP reanalysis data. We make the assumption that the large-scale dynamics in the NCEP system are sufficiently accurate to yield good estimates of the free-tropospheric subsidence above the inversion capping the MBL top. We use MODIS and TMI observations to determine the climatological mean boundary layer depth and the downstream deepening in the entrainment-rate equation.

Mean entrainment rates in the regions free of strong surface forcing are in the range 2–6 mm s^{-1}, and are found to be 0%–30% greater than the local subsidence rates. These entrainment rates do not depend strongly upon the climatological cloud amount, probably because a downstream reduction in turbulence is offset by a weaker inversion in the stratocumulus to cumulus tran-

sition. Instead, the balance in most areas is between the entrainment and the radiatively driven subsidence above the MBL.

A novel method is presented to make estimates of boundary layer decoupling by combining satellite, reanalysis, and climatological datasets. The boundary layer moisture profile is found to be stratified (decoupled), and the stratification increases with increasing MBL depth. When the boundary layer is shallower than 500–700 m, little decoupling is evident, consistent with the mixed-layer model analysis and theory of Bretherton and Wyant (1997). Values of the moisture-decoupling parameter agree well with radiosonde data, although some regional differences may suggest that other factors such as downstream deepening of the MBL, or drizzle, may also play a role in setting the degree of decoupling.

When the MBL is deeper than approximately 1 km, mixed-layer assumptions lead to physical inconsistencies with cloud thicknesses and liquid water paths that are significantly larger than those observed. However, the mixed-layer approach may be a useful framework to examine the relationship between turbulence, inversion strength, and entrainment rate using a combination of remote sensing and reanalysis. We plan to examine this issue in our future work.

Acknowledgments. MODIS data used in this study are provided by the NASA GES Distributed Active Archive Center. TMI data are produced by Remote Sensing Systems and sponsored, in part, by NASA's Earth Science Information Partnerships (ESIP): a federation of information sites for earth science; and by the NOAA/NASA Pathfinder Program for early EOS products; principal investigator: Frank Wentz. QuikSCAT data are produced by Remote Sensing Systems and sponsored by the NASA Ocean Vector Winds Science Team. EPIC was funded by NOAA and NSF. Dynamics and Chemistry of Marine Stratocumulus (DYCOMS-2) was funded by NSF. Funding for this work was provided by the NASA EOS Grant NAGS5-10624 Climate Processes over the Oceans. We are grateful to Bjorn Stevens and an anonymous reviewer for insightful and constructive criticism.

APPENDIX

Uncertainties in Inversion Height, Subsidence, Entrainment and Decoupling

The estimation of z_i involves the solution of the rather complicated Eq. (6) for each of the MODIS scenes. We carry out an error analysis on the estimated values of z_i. To do this we assign errors in the input parameters based upon our best estimation of the likely uncertainties inherent in observation/reanalysis/COADS. Both bias and random errors are considered separately. For each input parameter, we construct ''erroneous'' input parameters and then derive erroneous z_i values for all the MODIS scenes. A mean bias and an rms difference is then obtained for each input parameter, and these statistics are subclassified by z_i.

The input parameters considered are θ_0, θ_{700}, $\Gamma_{\rm FT}$, $T_{\rm top}$, $q_{T,0}$, q_{700}, $z_{\rm ML}$, LWP, and cloud fraction (CF). Other parameters, such as p_0 do not contribute significantly to any error in z_i. Estimated errors in input parameters are summarized in Table A1 and are discussed briefly in the following paragraphs.

a. Uncertainty in basic parameters

1) Surface and 700-hPa potential temperature, and $\Gamma_{\rm FT}$

The uncertainty in θ_0 stems from uncertainty in SST and in ΔT_{S-A}. Sea surface temperature from the TMI shows random errors of around 0.5 K when compared to buoy data, with mean biases that are significantly smaller than this (see www.remss.com). Because we use constant location-dependent COADS climatologies of ΔT_{S-A} we can expect some error here. Over much of the subtropics the mean and the variability in ΔT_{S-A} is quite small [0.8-K mean and 0.5-K standard deviation for September–October 2000 at the Weller Buoy [20°S, 85°W], and so we would not expect the differences between the true values of ΔT_{S-A} and COADS values to be greater than around 0.5 K. We therefore estimate an error in θ_0 of 1 K.

EPIC radiosonde ascents are compared with coincident NCEP reanalysis data to assess the uncertainties in θ_{700}. NCEP tended to overestimate θ_{700} with a mean bias of 1.3 K and an rms difference of around 1.6 K. NCEP most likely performs better in the NE Pacific but we assign an error of approximately 2 K as a general estimate for both regions in this study.

A number of data sources are available to examine the variability in $\Gamma_{\rm FT}$. Composite radiosonde profiles from Albrecht et al. (1995) in several subtropical and tropical locations suggest that our choice of $\Gamma_{\rm FT} = 5$ K km^{-1} is likely to introduce a location-dependent bias of around 1 K km^{-1}. The temporal variability of $\Gamma_{\rm FT}$ at a fixed subtropical location (20°S, 85°W) during the EPIC field campaign (Bretherton et al. 2003) was approximately 1 K km^{-1}.

2) Cloud-top temperature

We performed a comparison between radiosonde-derived $T_{\rm top}$ from the EPIC field campaign and coincident MODIS-derived $T_{\rm top}$ in cases where only MBL clouds were present. The rms difference between the two measurements was 0.35 K, with an even smaller bias, but we estimate the standard error in $T_{\rm top}$ to be somewhat higher (1 K) than this because the EPIC location (20°S, 85°W) has among the lowest water vapor paths above the MBL (2–5 mm) of the regions in this study. The error in $T_{\rm top}$ is expected to increase in regions with moister and/or more variable tropospheric moisture contents.

TABLE A1. Propagated mean bias and rms errors in z_i for the stated bias errors in each input parameter. Data are subdivided by z_i range, including the final column which is for all z_i. Also shown is the rms error in z_i assuming random errors in *all* parameters with standard error equal to the values given in the second column.

Input parameter	Error	z_i in range: 0–1000 m	1000–1500 m	1500–2000 m	2000–2500 m	All z_i
		Bias errors in z_i (m):				
θ_0	1 K	125	119	102	84	108
θ_{700}	2 K	40	75	97	145	90
Γ_{FT}	1 K km^{-1}	16	−14	−39	−15	−19
T_{top}	1 K	−107	−124	−144	−181	−138
q_{700}	2 g kg^{-1}	46	81	103	200	105
$q_{T,0}$	1 g kg^{-1}	100	88	69	66	78
z_{ML}	100 m	22	23	15	14	18
LWP	30 g m^{-2}	51	54	47	42	49
CF	0.1	27	27	15	2	19
		Overall rms error in z_i (m):				
Errors in all parameters		215	225	252	323	252
		Other bias errors in z_i (m):				
Assume mixed layer		−190	−441	−666	−1060	−570

3) SURFACE AND 700-HPA MIXING RATIO

Uncertainty in $q_{T,0}$ reflects uncertainty in the COADS surface humidity and in the SST. We estimate rms uncertainties in $q_{T,0}$ to be no greater than 1 g kg^{-1}.

Comparison of radiosonde ascents during the EPIC SE Pacific field campaign with NCEP reanalysis data shows that NCEP tends to overestimate the specific humidity at 700 hPa by 2 g kg^{-1} in the mean, with an rms error of around 2.6 g kg^{-1}. For DYCOMS-2 in the NE Pacific stratocumulus region (Stevens et al. 2003b), we find a considerably smaller NCEP bias (<0.5 g kg^{-1}) and rms (1 g kg^{-1}). Typical $q_T(z_i^+)$ is 1–2 g kg^{-1} for EPIC and 2–5 g kg^{-1} for DYCOMS-2 data, so the relative biases are 100% for EPIC and 10%–20% for DYCOMS-2.

4) SML DEPTH

The main source of error in the depth of the SML z_{ML} is the surface relative humidity RH_0, with the surface temperature being a very minor contributor. An uncertainty of 1% in RH_0 leads to an approximately 20–25-m error in z_{ML}. Typical monthly relative humidity standard deviation from COADS in the subtropical and tropical MBL is around 4% rising to around 8% closer to the storm tracks. Because we have selected only MODIS scenes containing exclusively warm cloud, we expect that the z_{ML} uncertainty attributable to using COADS data is approximately 150 m.

5) LIQUID WATER PATH AND CLOUD FRACTION

For individual scenes, the LWP observations from MODIS agree with spaceborne microwave radiometer estimates to within around 30 g m^{-2} (see, e.g., Wood et al. 2002), with biases of less than 5 g m^{-2} in the mean values. Using an upward-pointing microwave radiometer (MWR) LWP measurements (more accurate than satellite because of the cold background) from EPIC, we find that the rms difference between MODIS (8 km × 8 km means around the ship) and MWR LWP is 28 g m^{-2}, with a bias of only a few g m^{-2}. Thus, we

TABLE A2. As in Table A1 but for the decoupling parameter $\boldsymbol{\alpha}_q$.

Input parameter	Error	z_i in range: 0–1000 m	1000–1500 m	1500–2000 m	2000–2500 m	All z_i
		Bias errors in α_q:				
θ_0	1 K	−0.02	−0.02	−0.01	−0.01	−0.01
θ_{700}	2 K	−0.01	−0.01	−0.01	−0.01	−0.01
Γ_{FT}	1 K km^{-1}	<0.01	<0.01	<0.01	<0.01	<0.01
T_{top}	1 K	−0.08	−0.06	−0.05	−0.04	−0.05
q_{700}	2 g kg^{-1}	−0.02	0.04	0.08	0.16	0.07
$q_{T,0}$	1 g kg^{-1}	−0.02	−0.01	−0.01	−0.01	−0.01
z_{ML}	100 m	<0.01	<0.01	<0.01	<0.01	<0.01
LWP	30 g m^{-2}	−0.03	−0.02	−0.02	−0.02	−0.02
CF	0.1	<0.01	<0.01	<0.01	<0.01	<0.01
		Overall rms error in α_q:				
Errors in all parameters		0.11	0.09	0.10	0.13	0.13

can conclude that the errors for each estimate are of the order of 30 g m^{-2}.

Comparison of MODIS cloud fractions with International Satellite Cloud Climatology Project (ISCCP) show differences of 0.05–0.2 throughout the subtropics and Tropics. Although one would expect that MODIS would be somewhat more accurate than ISCCP because of the improved cloud mask, we assign an error of 0.2.

b. Uncertainty in z_i

The z_i error analysis (Table A1) reveals that the most important contributors to the overall uncertainty in z_i are the cloud-top temperature T_{top}, and the surface potential temperature. These are the dominant uncertainties over the entire z_i range, although for the deeper MBLs other sources of uncertainty, such as θ_{700} are as dominant. This is because as the MBL becomes deeper, and more decoupled, the free-tropospheric parameters become more important in the determination of z_i. Uncertainties in z_{ML}, LWP, and CF do not contribute strongly to the overall error in z_i.

If we assume that the assigned errors are random and uncorrelated, we can estimate the expected rms error in z_i from the combination of the input parameter errors. These are presented in Table A1 and range from 200 m for the shallowest to 375 m for the deepest ($z_i > 2000$ m) MBLs. When gridded, these random errors will translate into errors in the mean z_i for each $5^\circ \times 5^\circ$ subregion ranging from 25 m in the shallow MBL regions near the coasts to 75 m in the trade wind and equatorial regions. These errors are relatively small compared with the variation in mean z_i across the regions of interest.

We can also examine the uncertainties related to the choice of model used to describe the MBL thermodynamic structure by comparing with the z_i values that are derived if the MBL is assumed to be well mixed (i.e., have a constant θ_L profile). This analysis reveals (Table A1) that assuming a mixed layer leads to mean z_i values that range from 200 m lower than the PLR values (for shallow z_i) to 600–1000 m lower (for deep z_i). For the intermediate and deeper MBLs, these values are larger than the uncertainties related to incomplete knowledge of the input parameters.

The September–October 2000 median z_i values using the PLR formulation are within 75 m of the mean MBL depth at 20°S, 85°W measured during EPIC in October 2001. We hope to extend our estimates to other locations and seasons so that we can compare directly with other in situ observations in the future.

c. Uncertainty in w_s

To examine the credibility of the derived subsidence rates we also estimate $D = \partial u/\partial x + \partial v/\partial y$ from the NCEP surface wind data corresponding to the MODIS scene, which we compare with the surface divergence rates from NASA Quick Scatterometer (QuikSCAT). QuikSCAT data are taken from the daily product from Remote Sensing Systems. If NCEP is producing the correct surface divergences it provides some confidence in its estimation of the subsidence rates, although we note that disagreement between reanalysis and QuikSCAT could arise from problems with the NCEP boundary layer scheme, rather than problems with the large-scale dynamics. Over much of the NE Pacific subtropics the rms difference between the QuikSCAT and NCEP $2.5^\circ \times 2.5^\circ$ 2-month mean surface divergences are 30% of the mean. In the SE Pacific, these differences are closer to 50%. For the regions as a whole, the mean biases are around 10%–15% (with QuikSCAT D larger than NCEP in the NE Pacific, and smaller in the SE Pacific), and much of the rms difference may be related to statistical noise in the QuikSCAT/NCEP due to D being a derivative field. The estimated sampling error in the mean divergence for each $2.5^\circ \times 2.5^\circ$ region is 10%–60%, depending upon the number of scenes in each region. For the regions with the sampling error less than 30%, the rms Quikscat-NCEP differences fall to around 20% in the NE Pacific and 35% in the SE Pacific. We conclude that these figures are representative of the uncertainties in the $2.5^\circ \times 2.5^\circ$ 2-month mean 850-hPa NCEP subsidence rates.

d. Uncertainty in downstream deepening

Error in the magnitude of $\overline{\mathbf{u}(z_i) \cdot \nabla z_i}$ is dependent upon the uncertainties is the mean inversion-level winds, the uncertainty in the mean z_i gradient, and the relative magnitude of the eddy term $\overline{\mathbf{u}'(z_i) \cdot \nabla z_i'}$. The noise in the estimations of z_i for each scene (see earlier) preclude the use of the data to examine the magnitude of the eddy term. For the uncertainty in the mean z_i gradient, assuming that the biases in z_i are larger for deeper MBLs and are as large as those assuming a mixed layer (Table A1), we might expect the relative error in the mean z_i gradient between coastal California and the trade winds to be approximately 30%, but will be smaller (larger) in regions of shallower (deeper) z_i. It is not possible to make further quantitative inferences about the downstream deepening errors with the data currently available.

e. Uncertainty in $\overline{w_e}$

Over much of subtropics and Tropics, the uncertainty in $\overline{w_e}$ will be probably be dominated by uncertainty in $\overline{w_s(z_i)}$ because the downstream deepening term in (3) is small. We estimate an uncertainty in $\overline{w_e}$ of at least 25% in the NE Pacific and 40% in the SE Pacific. These are a little greater than the uncertainties in entrainment rates estimated using either in situ aircraft flux measurements (e.g., FAL) and intensive budget studies (P. Caldwell et al., 2004, unpublished manuscript), but have the advantage of being considerably more representative of

the cloud-capped MBL over large time and space scales. The uncertainties will decrease as reanalyses improve in quality.

f. Uncertainty in α_q

Uncertainties in α_q arise from both the model assumptions and uncertainties in the parameters required by the model to determine z_i and α_q.

We make the assumption in this study that the decoupling parameters for q_T and θ_L are related (see section 2b). Whether or not this rigid relationship holds in reality is uncertain. This constraint seems physically realistic if the air in the layer between the top of the SML and the MBL inversion is assumed to be the result of mixing of SML and above-inversion air.

Table A2 is equivalent to Table A1 but for α_q errors. Uncertainties in α_q are dominated by uncertainty in T_{top} and, at larger z_i, in q_{700}. Overall, our best guess at an rms uncertainty in α_q is approximately 0.1–0.13 per scene, with only a weak dependence upon z_i. Because bias errors are likely to contribute significantly to these errors, we estimate that the averaging of scenes to reduce sampling uncertainty may not significantly reduce these uncertainties.

REFERENCES

Albrecht, B. A., M. P. Jensen, and W. J. Syrett, 1995: Marine boundary layer structure and fractional cloudiness. *J. Geophys. Res.,* **100,** 14 209–14 222.

Betts, A. K., 1985: Mixing line analysis of clouds and cloudy boundary layers. *J. Atmos. Sci.,* **42,** 2751–2763.

——, and B. A. Albrecht, 1987: Conserved variable analysis of the convective boundary layer thermodynamic structure over the tropical oceans. *J. Atmos. Sci.,* **44,** 83–99.

——, and W. Ridgway, 1988: Coupling of the radiative, convective, and surface fluxes over the equatorial Pacific. *J. Atmos. Sci.,* **45,** 522–536.

——, P. Minnis, W. Ridgway, and D. Young, 1992: Integration of satellite and surface data using a radiative–convective oceanic boundary layer model. *J. Appl. Meteor.,* **31,** 340–350.

——, C. S. Bretherton, and E. Klinker, 1995: Relation between mean boundary-layer structure and cloudiness at the *R/V Valdivia* during ASTEX. *J. Atmos. Sci.,* **52,** 2752–2762.

Bolton, D., 1980: The computation of equivalent potential temperature. *Mon. Wea. Rev.,* **108,** 1046–1053.

Bretherton, C. S., and R. Pincus, 1995: Cloudiness and marine boundary layer dynamics in the ASTEX Lagrangian experiments. Part I: Synoptic setting and vertical structure. *J. Atmos. Sci.,* **52,** 2707–2723.

——, and M. C. Wyant, 1997: Moisture transport, lower-tropospheric stability, and decoupling of cloud-topped boundary layers. *J. Atmos. Sci.,* **54,** 148–167.

——, T. Uttal, C. W. Fairall, S. E. Yuter, R. A. Weller, D. Baumgardner, K. Comstock, and R. Wood, 2003: The EPIC 2001 stratocumulus study. *Bull. Amer. Meteor. Soc.,* **85,** 967–977.

Deardorff, J. W., 1976: On the entrainment rate of a stratocumulus topped mixed layer. *Quart. J. Roy. Meteor. Soc.,* **102,** 563–582.

de Roode, S. R., and P. G. Duynkerke, 1997: Observed Lagrangian transition of stratocumulus into cumulus during ASTEX: Mean state and turbulence structure. *J. Atmos. Sci.,* **54,** 2157–2173.

deSzoeke, S. P., and C. S. Bretherton, 2004: Quasi-Lagrangian large eddy simulations of cross-equatorial flow in the east Pacific atmospheric boundary layer. *J. Atmos. Sci.,* **61,** 1837–1858.

Garreaud, R. D., J. Rutllant, J. Quintana, J. Carrasco, and P. Minnis, 2001: Cimar-5: A snapshot of the lower troposphere over the subtropical southeast Pacific. *Bull. Amer. Meteor. Soc.,* **82,** 2193–2207.

Heck, P. W., B. J. Byars, D. F. Young, P. Minnis, and E. F. Harrison, 1990: A climatology of satellite derived cloud properties over marine stratocumulus regions. Preprints, *Conf. on Cloud Physics,* San Francisco, CA, Amer. Meteor. Soc., J1–J7.

King, M. D., Y. Kaufman, W. P. Menzel, and D. Tanré, 1992: Remote sensing of cloud, aerosol, and water vapor properties from the Moderate Resolution Imaging Spectroradiometer (MODIS). *IEEE Trans. Geosci. Remote Sens.,* **30,** 2–27.

——, S.-C. Tsay, S. E. Platnick, M. Wang, and K.-N. Liou, 1997: Cloud retrieval algorithms for MODIS: Optical thickness, effective particle radius, and thermodynamic phase. MODIS Algorithm Theoretical Basis Document ATBD-MOD-05, NASA, 78 pp.

Kistler, R., and Coauthors, 2001: The NCEP–NCAR 50-year reanalysis: Monthly means CD–ROM and documentation. *Bull. Amer. Meteor. Soc.,* **82,** 247–267.

Klein, S. A., 1997: Synoptic variability of low-cloud properties and meteorological parameters in the subtropical trade wind boundary layer. *J. Climate,* **10,** 2018–2039.

Kloesel, K. A., 1992: A 70-year history of marine stratocumulus cloud field experiments off the coast of California. *Bull. Amer. Meteor. Soc.,* **73,** 1581–1585.

Kummerow, C., W. Barnes, T. Kozu, J. Shiue, and J. Simpson, 1998: The Tropical Rainfall Measuring Mission (TRMM) sensor package. *J. Atmos. Oceanic Technol.,* **15,** 809–817.

Lilly, D. K., 1968: Models of cloud-topped mixed layers under a strong inversion. *Quart. J. Roy. Meteor. Soc.,* **94,** 292–309.

McGauley, M, C. Zhang, and N. Bond, 2004: Large-scale characteristics of the atmospheric boundary layer in the eastern Pacific cold tongue–ITCZ region. *J. Climate,* in press.

Minnis, P., P. W. Heck, D. F. Young, C. W. Fairall, and J. B. Snider, 1992: Stratocumulus cloud properties derived from simultaneous satellite and island-based instrumentation during fire. *J. Appl. Meteor.,* **31,** 317–339.

Nakajima, T., and M. D. King, 1990: Optical thickness and effective particle radius of clouds from reflected solar radiation measurements. Part I: Theory. *J. Atmos. Sci.,* **47,** 1878–1893.

Neiburger, M., D. S. Johnson, and C. W. Chien, 1961: *Part 1: The Inversion over the Eastern North Pacific Ocean. Studies of the Structure of the Atmosphere over the Eastern Pacific Ocean in Summer, Univ. of California Publications in Meteor.,* No. 1, University of California Press, 1–94.

Nicholls, S., and J. D. Turton, 1986: An observational study of the structure of stratiform cloud sheets: Part II. Entrainment. *Quart. J. Roy. Meteor. Soc.,* **112,** 461–480.

Osborne, S. R., and Coauthors, 2000: Evolution of the aerosol, cloud and boundary-layer dynamic and thermodynamic characteristics during the 2nd Lagrangian experiment of ACE-2. *Tellus,* **52B,** 375–400.

Riehl, H., T. C. Yeh, J. S. Malkus, and N. E. LaSeur, 1951: The northeast trade of the Pacific Ocean. *Quart. J. Roy. Meteor. Soc.,* **77,** 598–626.

Stevens, B., 2003: Entrainment in stratocumulus topped mixed layers. *Quart. J. Roy. Meteor. Soc.,* **128,** 2663–2690.

——, and Coauthors, 2003a: On entrainment rates in nocturnal marine stratocumulus. *Quart. J. Roy. Meteor. Soc.,* **129,** 3469–3493.

——, and Coauthors, 2003b: Dynamics and Chemistry of Marine Stratocumulus—DYCOMS II. *Bull. Amer. Meteor. Soc.,* **84,** 579–593.

Thum, N., S. K. Esbensen, D. B. Chelton, and M. J. McPhaden, 2002: Air–sea heat exchange along the northern sea surface temperature front in the eastern tropical Pacific. *J. Climate,* **15,** 3361–3378.

von Ficker, H., 1936: Die Passatinversion. Meteorological Institute, University of Berlin, 36 pp.

Wakefield, J. S., and W. H. Schubert, 1981: Mixed-layer model simulation of eastern North Pacific stratocumulus. *Mon. Wea. Rev.*, **109,** 1952–1968.

Wang, S., B. A. Albrecht, and P. Minnis, 1993: A regional simulation of marine boundary layer clouds. *J. Atmos. Sci.*, **50,** 4022–4043.

Wentz, F. J., 1997: A well calibrated ocean algorithm for special sensor microwave/imager. *J. Geophys. Res.*, **102,** 8703–8718.

Wood, R., and J. P. Taylor, 2001: Liquid water path variability in unbroken marine stratocumulus. *Quart. J. Roy. Meteor. Soc.*, **127,** 2635–2662.

——, C. S. Bretherton, and D. L. Hartmann, 2002: Diurnal cycle of liquid water path over the subtropical and tropical oceans. *Geophys. Res. Lett.*, **29,** 2092, doi:10.1029/2002GL015371.

Woodruff, S. D., H. F. Diaz, J. D. Elms, and S. J. Worley, 1998: COADS Release 2 data and metadata enhancements for improvements of marine surface flux fields. *Phys. Chem. Earth*, **23,** 517–527.